Effect of Hubbard U on the construction of low-energy Hamiltonians for $LaMnO_3$ via maximally localized Wannier functions

Roman Kováčik* and Claude Ederer
School of Physics, Trinity College Dublin, Dublin 2, Ireland
(Received 8 April 2011; published 8 August 2011)

We use maximally localized Wannier functions to construct tight-binding (TB) parametrizations for the e_g bands of $LaMnO_3$ based on first-principles electronic structure calculations. We compare two different ways to represent the relevant bands around the Fermi level: (i) a *d-p model* that includes atomic-like orbitals corresponding to both Mn(d) and O(p) states in the TB basis, and (ii) an *effective e_g model* that includes only two e_g-like Wannier functions per Mn site. We first establish the effect of the Jahn-Teller distortion within the d-p model, and then compare the TB representations for both models obtained from GGA+U calculations with different values of the Hubbard parameter U. We find that in the case of the d-p model the TB parameters are rather independent of the specific value of U, if compared with the mean-field approximation of an appropriate multiband Hubbard Hamiltonian. In contrast, the U dependence of the TB parameters for the effective e_g model cannot easily be related to a corresponding mean-field Hubbard model, and therefore these parameters depend critically on the specific value of U, and more generally on the specific exchange-correlation functional, used in the electronic structure calculation.

DOI: 10.1103/PhysRevB.84.075118 PACS number(s): 71.10.−w, 71.27.+a, 71.70.Ej

I. INTRODUCTION

The construction of realistic low-energy Hamiltonians based on first-principles electronic structure calculations is an important tool for the investigation of correlated electron systems, such as cuprates, manganites, or other complex transition-metal (TM) oxides. While much of the general physics determining the diverse properties of these materials can be understood in terms of simplified models,[1–3] the corresponding model parameters are generally unknown and have to be adjusted to fit experimental data. Alternatively, electronic structure calculations based on density functional theory (DFT)[4,5] or quantum-chemical methods can be used to determine these parameters,[6–9] which in turn allows for a quantitative evaluation of the underlying model assumptions and the construction of realistic model Hamiltonians with all parameters determined *ab initio*.[10,11]

Model Hamiltonians for correlated electron systems are typically formulated within a tight-binding (TB) picture that involves only a small number of electronic states localized on certain atoms (e.g., the "d states" of the TM atoms within a TM oxide).[1–3] Ideally, these states give rise to an isolated group of bands around the Fermi energy, which then determines the low-energy behavior of the system. A corresponding TB representation can in principle be obtained by constructing Wannier functions from the Kohn-Sham Bloch states calculated within DFT.[11–16]

In the case of model Hamiltonians that contain an explicit electron-electron interaction, typically in the form of a local Hubbard term with interaction parameter U, the DFT band structure can either be viewed as mean-field approximation to this interacting model, or as representative for the "noninteracting" case, i.e., corresponding to $U = 0$ in the model Hamiltonian. While it is often convenient to consider the electronic structure calculated within either the local density approximation (LDA)[4,17] or the generalized gradient approximation (GGA)[18] as essentially noninteracting, this is probably not a good assumption if the electronic structure is calculated using more advanced exchange correlation functionals such as (LDA/GGA)+U or hybrid functionals.[19–21]

In this work we use maximally localized Wannier functions (MLWFs)[22–24] to obtain TB parametrizations for the important case of $LaMnO_3$, the parent material of the colossal magnetoresistive manganites, and a prototype system for correlated electron physics.[3,25] We calculate the electronic structure of $LaMnO_3$ using the GGA+U method and different values for the Hubbard parameter U. We then compare two different ways to represent the relevant bands around the Fermi level: (i) a *d-p model* that includes atomic-like orbitals corresponding to both Mn(d) and O(p) states in the TB basis, and (ii) an *effective e_g model* that includes only two e_g-like Wannier functions per Mn site. In particular, we analyze the U dependence of the two different TB parametrizations and relate this to commonly used model Hamiltonians for manganites.

We find that for the d-p parametrization, the effect of U is mostly local, leading to U-dependent shifts of the on-site energies and an increase in the Jahn-Teller (JT) splitting, whereas the corresponding hopping amplitudes are only weakly affected by the value of U. Thus, the U dependence of the d-p parameters closely resembles the U dependence of a corresponding multiband Hubbard Hamiltonian in mean-field approximation. On the other hand, the change of on-site energies and JT splitting for the effective e_g MLWFs, calculated for different values of U, are distinctly different from a corresponding mean-field model Hamiltonian. In addition, there is also a strong U dependence of the effective e_g hopping amplitudes, which is due to electronic degrees of freedom that are excluded from the TB basis. This indicates that while the TB parametrization for the d-p model is fairly robust with respect to a variation of U, for the case of the effective e_g basis an appropriate choice of U in the GGA+U calculation is crucial. Our results demonstrate the simple fact that the transferability of a specific TB parametrization is generally increased if more electronic degrees of freedom are included in the model description.

This paper is organized as follows. In the next section we first summarize the most important aspects of typical model Hamiltonians for manganites, emphasizing in particular the role of the JT distortion (Sec. II A), before introducing MLWFs (Sec. II B) and describing the technical details of our calculations (Sec. II C). In Secs. III A and III B we first present the main features of the d-p model based on the MLWFs calculated for $U = 0$ eV, and then clarify the effect of the JT distortion on the corresponding TB parameterization. An analogous analysis for the effective e_g model parametrization has recently been presented in Ref. 11. The effect of varying the Hubbard U in the GGA+U calculation on the MLWF parameters of the two different models is presented in Sec. III C for the d-p model and in Sec. III D for the effective e_g model. Finally, Sec. IV summarizes our main conclusions, while further details about the d-p TB parametrization can be found in the Appendix.

II. METHOD AND THEORETICAL BACKGROUND

A. Jahn-Teller distortion in $LaMnO_3$

$LaMnO_3$ crystallizes in an orthorhombically distorted perovskite structure with $Pbnm$ space group symmetry.[26] The distortion relative to the cubic perovskite structure can be decomposed into three components:[10] a staggered JT distortion of the MnO_6 octahedra, alternating tilts and rotations of these octahedra around the cubic axes ($GdFeO_3$ distortion), and an orthorhombic strain of the unit cell. The electronic structure of $LaMnO_3$ around the Fermi energy is dominated by Mn $3d$ states, which are split by the octahedral crystal field into lower lying t_{2g} and higher lying e_g states.[27–29] The formal d^4 occupation of the Mn^{3+} cation leads to a high-spin configuration with filled majority spin t_{2g} states, half-filled majority spin e_g states, and empty minority spin states. The low-energy behavior of $LaMnO_3$ is therefore governed by the partially filled majority spin bands with predominant e_g character.

Motivated by this, the complex phenomenology observed in manganites is often modeled within an effective TB model that involves only two e_g orbitals per Mn site. Electrons can then hop between the two e_g levels on neighboring sites, and can interact with each other through a Hubbard-type electron-electron interaction, with the t_{2g} "core spins" through a Hund's rule interaction, and with the local JT distortion through a crystal-field splitting (see, e.g., Ref. 3). It is usually understood that the corresponding "e_g orbitals" are spatially extended Wannier orbitals that result from hybridization between atomic-like Mn(e_g) orbitals and the p orbitals of the surrounding oxygen ligands.

The effect of the JT distortion on this e_g manifold is typically expressed via a local crystal-field splitting of the form

$$\hat{H}_{\mathrm{JT}} = -\lambda \sum_{\mathbf{R},\sigma,a,b,i} \hat{c}^{\dagger}_{a\mathbf{R}\sigma}\, Q^{i}_{\mathbf{R}}\, \tau^{i}_{ab}\, \hat{c}_{b\mathbf{R}\sigma}. \tag{1}$$

Here, λ is the JT coupling strength, $\boldsymbol{\tau}_{ab}$ are the usual Pauli matrices, $\hat{c}_{b\mathbf{R}\sigma}$ is the annihilation operator corresponding to orbital b with spin σ at site $\mathbf{R}$, and the JT distortion of the oxygen octahedron surrounding site $\mathbf{R}$ is described by specific modes $Q^{i}_{\mathbf{R}}$ ($i = x,z$).[3]

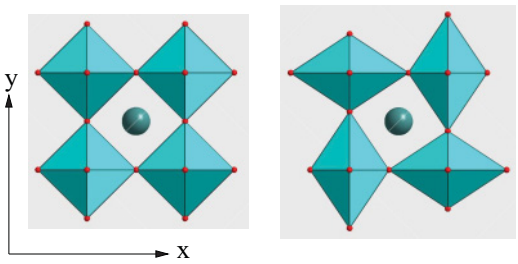

FIG. 1. (Color online) Left: Ideal cubic perovskite structure viewed along the z axis. Right: Staggered Q^x-type JT distortion within the x-y plane. Oxygen anions are shown as small (red) spheres, the La cation as a large (green) sphere. Mn cations (not shown) are situated in the middle of each oxygen octahedron.

In the following we only consider a staggered JT distortion of the form $Q^{x}_{\mathbf{R}} = -Q^{x}_{\mathbf{R}'}$, where $\mathbf{R}$ and $\mathbf{R}'$ correspond to nearest neighbor sites within the x-y plane (see Fig. 1). Thereby,

$$Q^{x}_{\mathbf{R}} = \frac{1}{\sqrt{2}}\left(d^{x}_{\mathbf{R}} - d^{y}_{\mathbf{R}}\right), \tag{2}$$

with $d^{x}_{\mathbf{R}}$ and $d^{y}_{\mathbf{R}}$ being the Mn-O distances along the x and y directions, respectively, corresponding to the oxygen octahedron surrounding the Mn at site $\mathbf{R}$. We note that it has been shown in Ref. 10 that this component of the JT distortion has the most pronounced effect on the electronic structure of $LaMnO_3$. Furthermore, in Ref. 11 we showed that the effect of the various structural distortions on the calculated model parameters can be analyzed separately, since they are to a great extent independent of each other.

B. Maximally localized Wannier functions

A set of N localized Wannier functions $|w_{n\mathbf{T}}\rangle$ corresponding to a group of N bands that are described by delocalized Bloch states $|\psi_{m\mathbf{k}}\rangle$ is defined by the following transformation:

$$|w_{n\mathbf{T}}\rangle = \frac{V}{(2\pi)^3}\int_{\mathrm{BZ}} d\mathbf{k}\left[\sum_{m=1}^{N} U^{(\mathbf{k})}_{mn}|\psi_{m\mathbf{k}}\rangle\right] e^{-i\mathbf{k}\cdot\mathbf{T}}. \tag{3}$$

Thereby, $\mathbf{T}$ is the lattice vector of the unit cell associated with the Wannier function, m is a band index, $\mathbf{k}$ is the wave vector of the Bloch function, and the integration is performed over the first Brillouin zone (BZ) of the lattice. Different choices for the unitary matrix $\mathbf{U}^{(\mathbf{k})}$ lead to different Wannier functions, which are thus not uniquely defined by Eq. (3). A unique set of *maximally localized Wannier functions* (MLWFs) can be generated by minimizing the total quadratic spread of the Wannier orbitals.[22]

Once the transformation matrices $\mathbf{U}^{(\mathbf{k})}$ are determined, a TB representation of the Hamiltonian in the MLWF basis is obtained:

$$\hat{H} = \sum_{\mathbf{T},\Delta\mathbf{T}} h^{\Delta\mathbf{T}}_{nm}\, \hat{c}^{\dagger}_{n\mathbf{T}+\Delta\mathbf{T}}\hat{c}_{m\mathbf{T}} + \mathrm{H.c.}, \tag{4}$$

with

$$h^{\mathbf{T}}_{nm} = \frac{V}{(2\pi)^3}\int_{\mathrm{BZ}} d\mathbf{k}\left[\sum_{l}\left(U^{(\mathbf{k})}_{ln}\right)^{*}\epsilon_{l\mathbf{k}}\, U^{(\mathbf{k})}_{lm}\right] e^{-i\mathbf{k}\cdot\mathbf{T}}. \tag{5}$$

Here, $\epsilon_{l\mathbf{k}}$ is the eigenvalue corresponding to Bloch function $|\psi_{l\mathbf{k}}\rangle$. For cases where the bands of interest do not form an isolated set of bands but are entangled with other bands, a two-step procedure for obtaining the unitary transformation matrices (which in this case are typically rectangular) is employed.[23]

We note that $\mathbf{T}$ and $\Delta\mathbf{T}$ in Eqs. (3)–(5) indicate lattice translations, whereas for crystal structures with more than one atom per unit cell n and m represent a combined orbital and site index, specifying the various orbitals at all sites within the primitive unit cell.

C. Computational details

All results presented in this work are obtained from spin-polarized first-principles DFT calculations using the QUANTUM ESPRESSO program package,[30] the GGA exchange-correlation functional of Perdew, Burke, and Ernzerhof,[18] and Vanderbilt ultrasoft pseudopotentials.[31] La $(5s,5p)$ and Mn $(3s,3p)$ semicore states are included in the valence. The Hubbard $+\,U$ correction is applied using the simplified approach according to Dudarev *et al.*,[20] which corresponds to the case $J = 0$ in the more elaborate expression by Lichtenstein *et al.*[19] Projections on orthogonalized atomic Mn(d) orbitals are used to evaluate the U-dependent contributions to potential and energy.

To analyze the effect of the JT distortion on the electronic structure of $LaMnO_3$, we perform GGA calculations with different degrees of distortion. Starting from the ideal cubic perovskite structure, we gradually increase the amplitude of the JT distortion $|Q^x_{\mathbf{R}}|$ from 0 to $Q^x_0 = 0.151$ Å. The latter value corresponds to the amount of distortion found in the experimentally observed crystal structure of $LaMnO_3$.[32] For the undistorted case we use a cubic perovskite structure with lattice constant $a_0 = 3.9345$ Å, which results in the same volume $V = 60.91$ Å^3 per formula unit as in the experimentally observed $Pbnm$ structure.[32]

After obtaining the DFT Bloch bands, we construct MLWFs using the WANNIER90 program integrated into the QUANTUM ESPRESSO package.[24] Starting from an initial projection of atomic d and p basis functions centered on the Mn and O sites onto the Bloch bands within an appropriately chosen energy window, we obtain sets of either 14 atomic-like (d-p model) or 2 more extended e_g-like (effective e_g model) MLWFs per spin channel and unit cell. In both cases we will in the following refer to the MLWF Hamiltonian matrix elements $h^{\mathbf{0}}_{nm}$ between the two different e_g-like MLWFs located on the same Mn site as *on-site off-diagonal element* q, to any matrix element between the same orbital at a particular site as *on-site energy* ε, and to matrix elements connecting two different sites as *hopping amplitudes* t. To assess the effect of the "$+U$" correction on the two different MLWF parametrizations we then construct the corresponding MLWFs for the fully JT distorted structure from GGA+U calculations with different values for the Hubbard U.

Convergence of the DFT total energy and total magnetization has been tested for the ideal cubic perovskite structure and ferromagnetic (FM) order. We find the total energy converged to an accuracy better than 1 mRy and the total magnetization converged to an accuracy of 0.05 μ_B for a plane-wave energy cutoff of 35 Ry and a Γ-centered $10 \times 10 \times 10$ k-point grid using a Gaussian broadening of 0.01 Ry. These values for plane-wave cutoff and Gaussian broadening are used throughout this work, whereas an appropriately reduced k-point grid of $7 \times 7 \times 10$ is used for the JT distorted structure with doubled unit cell in the x-y plane. The MLWFs are considered to be converged if the fractional change of the quadratic spread (both gauge-invariant and non-gauge-invariant part) between two successive iterations is smaller than 10^{-10}.

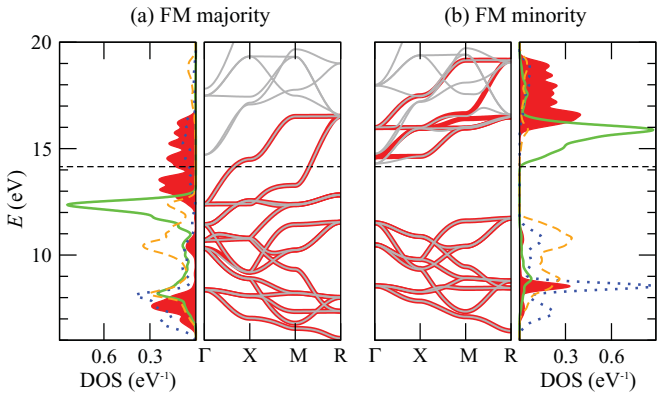

FIG. 2. (Color online) Projected DOS and band structure along high-symmetry lines within the BZ for cubic FM $LaMnO_3$. In the projected DOS plots, the filled (red) areas and solid (green) lines correspond to Mn(e_g) and Mn(t_{2g}) states, respectively, while dotted (blue) and dashed (orange) lines correspond to the O(p_σ) and O(p_π) states, respectively. In the band structure plots, the dispersion calculated from the MLWFs is represented by thick (red) lines. The Fermi level is indicated by the horizontal dashed lines.

III. RESULTS AND DISCUSSION

A. *d-p* TB parametrization for cubic $LaMnO_3$

In this section we establish the general features of the extended d-p TB description of $LaMnO_3$ within the ideal cubic perovskite structure, before we analyze the effect of the JT distortion in the next section. We are considering a FM arrangement of magnetic moments, but we have verified that the corresponding results for A-type antiferromagnetic (A-AFM) order do not exhibit any significant differences.

Figure 2 shows the projected densities of states (DOS) and band dispersion for both majority and minority spin channels. In agreement with previous calculations it can be seen that the majority spin DOS around the Fermi energy exhibit predominant Mn(e_g) orbital character, with Mn(t_{2g}) and O(p) bands located at slightly lower energies.[10,11,27,28] For minority spin, states with predominant Mn(e_g) and Mn(t_{2g}) character are located above the Fermi level. Strong hybridization between O(p) and Mn(d) orbitals is apparent from the various peaks in the DOS around 8 eV.

We construct 14 MLWFs per spin channel from the Kohn-Sham states located within an energy window of 3–17 eV and 3–20 eV for majority and minority spin, respectively. This corresponds to a TB representation of $LaMnO_3$ containing 5 Mn(d) orbitals and 9 O(p) orbitals per unit cell (three p orbitals corresponding to each of the three oxygen atoms within the simple cubic perovskite unit cell). The resulting MLWFs are depicted in Fig. 3. Three of the O(p) orbitals (one on each O atom) are pointing toward the Mn atom

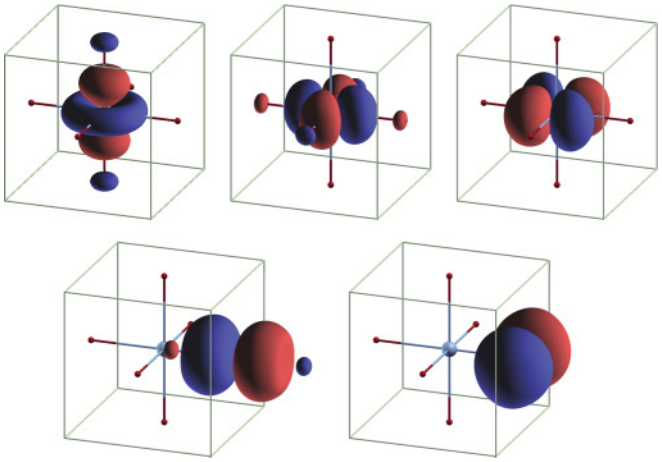

FIG. 3. (Color online) Real-space representation of the MLWFs corresponding to the d-p parametrization (FM, majority spin). Depicted are Mn($3z^2 - r^2$), Mn($x^2 - y^2$), and Mn(xy) MLWFs (top row from left to right), as well as two examples of O(p_σ) and O(p_π) orbitals (bottom row). The isosurface shown corresponds to a value of $\pm 1/\sqrt{V}$ where V is the unit cell volume. Picture generated using XCRYSDEN.[33]

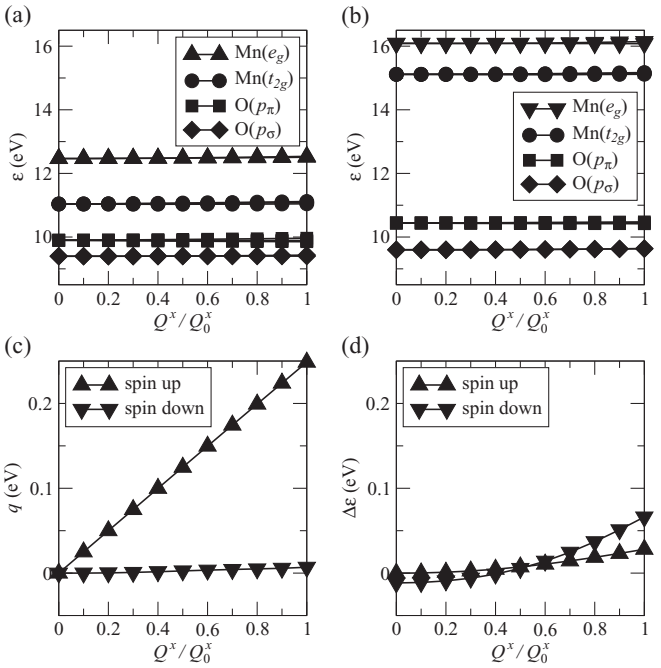

FIG. 4. On-site MLWF matrix elements of the d-p model as function of the JT distortion. (a) and (b) On-site energies for majority/minority spin. (c) On-site off-diagonal element q. (d) Splitting $\Delta\varepsilon$ between on-site energies of the two e_g-like MLWFs.

and hybridize with the Mn(e_g) orbitals. We call them O(p_σ) orbitals. The remaining 6 O(p) orbitals (two on each O atom) are oriented perpendicular to the Mn-O bond and hybridize with the Mn(t_{2g}) orbitals. These will be called O(p_π) orbitals in the following.

The MLWF bands [shown as thick (red) lines in Fig. 2] are identical to the corresponding DFT bands for majority spin, whereas for minority spin the MLWF and DFT bands above the Fermi energy exhibit certain differences which are due to the strong entanglement with other bands in that energy region.

From the real-space Hamiltonian matrix elements in the MLWF basis, Eq. (5), we find that the most dominant hopping corresponds to the shortest Mn-O and O-O bonds (see Fig. 10), but that a variety of other hopping amplitudes are also nonnegligible. In the following we will focus on the nearest neighbor Mn-O hopping amplitudes ($t_{eg,p\sigma}$ and $t_{t2g,p\pi}$) and analyze how they are affected by the JT distortion and the inclusion of a Hubbard U in the DFT calculations. A more detailed discussion of the d-p TB parameterization for cubic $LaMnO_3$ can be found in the Appendix.

B. Effect of JT distortion on the d-p TB parametrization

We now analyze the effect of the JT distortion on the on-site energies and nearest neighbor hopping parameters of the d-p model. As in the previous section, we will discuss only results for FM order as we do not find significant differences for the case of A-AFM order.

Figure 4 shows the diagonal on-site energies ε corresponding to Mn(e_g), Mn(t_{2g}), O(p_π), and O(p_σ) MLWFs, as well as the on-site off-diagonal matrix elements q between the two Mn(e_g) orbitals on the same site as a function of the JT amplitude Q^x/Q_0^x. It can be seen that the on-site energies for the various orbitals are essentially unaffected by the JT distortion. The corresponding changes, which lead to small differences between formerly symmetry-equivalent orbitals (see below for the case of the two e_g-like MLWFs), are of the order of a few tens of meV, and are thus negligible compared to the e_g-t_{2g} splitting or the d-p energy separation.

A more distinct effect of the JT distortion can be seen in the on-site off-diagonal matrix element q between the two majority spin Mn(e_g) orbitals on the same site. This matrix element is zero for the undistorted structure, but exhibits a linear increase to a value of about 0.25 eV for full JT distortion. This is consistent with the usual crystal-field picture of e_g orbitals in an octahedral environment [see also Eq. (1)]:[34] Within a $\{|3z^2 - r^2\rangle, |x^2 - y^2\rangle\}$ orbital basis, the Q^x-type JT distortion gives rise to a nonzero off-diagonal matrix element that increases linearly with the JT distortion, while the diagonal elements of the Hamiltonian remain constant.

However, the effect of the JT distortion observed for the minority spin q is significantly weaker than for the majority spin case. In fact, it is of similar magnitude as the small splitting between the corresponding diagonal matrix elements (on-site energies) $\Delta\varepsilon = \varepsilon[\text{Mn}(3z^2 - r^2)] - \varepsilon[\text{Mn}(x^2 - y^2)]$. We thus define a total JT-induced orbital splitting within the "e_g" orbital subspace as the difference in eigenvalues of the corresponding 2×2 on-site Hamiltonian matrix, which is given by $\delta = \sqrt{\Delta\varepsilon^2 + 4q^2}$. From the results presented in Fig. 4 for full JT distortion, i.e., $Q^x/Q_0^x = 1$, we obtain $\delta_\uparrow = 0.50$ eV for majority spin and $\delta_\downarrow = 0.07$ eV for minority spin.

To understand this large difference between majority and minority spin, we note that in a partially covalent system like $LaMnO_3$, the JT-induced orbital splitting is caused by a superposition of two effects: (i) the true (electrostatic) crystal-field effect, and (ii) a "ligand-field" effect due to changes in hybridization with the surrounding ligand orbitals. While the pure electrostatic crystal-field effect is identical for both spin projections, the hybridization with the surrounding

ligand orbitals is different for majority and minority spin orbitals, due to their large energy difference of about 3–4 eV.

In order to verify whether the large difference between majority and minority spin JT splitting is indeed due to a strong ligand-field contribution, we have constructed an alternative set of 20 MLWFs per formula unit and spin channel, where we explicitly included also the bands corresponding to O(s) and semicore La($5p$) states. These states are energetically lower than the Mn(d) and O(p) bands shown in Fig. 2, and are centered around $E \approx -3$ eV [La($5p$)] and $E \approx -5$ eV [O(s)]. The inclusion of these states in the MLWF basis reduces the "tails" in the e_g-like MLWFs located at surrounding O and La atoms, and should therefore decrease the ligand-field contribution to the local JT splitting. Indeed, we obtain $\delta_{\uparrow/\downarrow} = 0.36/0.12$ eV in this case; i.e., the spin-dependent ligand-field contribution to the JT splitting is indeed significantly reduced compared to the d-p MLWFs. The remaining difference can be ascribed to further contributions of orbitals that are not included in the MLWF basis and to the remaining small O(s), O(p), and La(p) contributions on the surrounding sites, which are required to ensure orthogonality between the MLWFs.

We also note that the JT splitting corresponding to the rather localized e_g MLWFs of the d-p TB model (0.50 eV for majority spin) is a factor of two smaller than the corresponding splitting for the more spatially extended MLWFs of the effective e_g model which was reported in Ref. 11 (0.97 eV for majority spin). This demonstrates the much stronger ligand-field effect in the less localized effective e_g MLWFs.

Next, we analyze the effect of the JT distortion on the nearest neighbor hopping between Mn(d) and O(p) orbitals. Figure 5 shows the corresponding changes in the majority spin hopping amplitudes (the results for minority spin do not exhibit any qualitative differences).

We first discuss hopping between Mn(t_{2g}) and O(p_π) orbitals [Fig. 5(a)]. It can be seen that the hopping amplitude $t_{t2g,p\pi}$ splits essentially according to the different Mn-O bond lengths in the JT distorted structure. The hopping amplitudes along the short (long) Mn-O bonds within the x-y plane

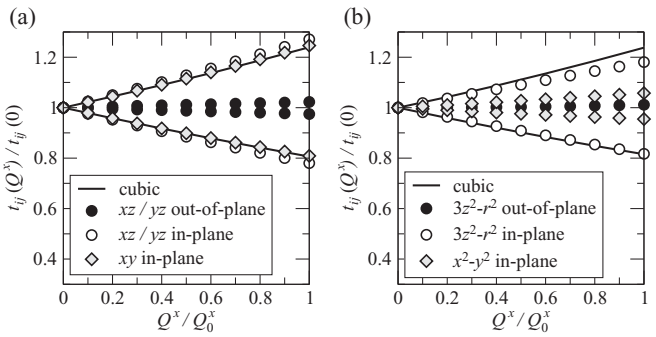

FIG. 5. Effect of increasing JT distortion on the hopping amplitudes $t_{t2g,p\pi}$ (a) and $t_{eg,p\sigma}$ (b) between Mn(d) and O(p) nearest neighbor orbitals (symbols). The different hopping amplitudes are denoted via the corresponding Mn(d) orbital and the direction of the hopping ("in-plane" corresponds to x-y directions, "out-of-plane" to the z direction). The solid lines correspond to the hopping amplitudes for a perfect cubic perovskite structure with lattice constant $a = a_0 \pm \Delta a$, where $\Delta a = \sqrt{2}Q^x$. Upper/lower branches correspond to short/long Mn-O bonds.

increase (decrease) with increasing JT distortion, while the hopping along the z direction, i.e., corresponding to constant Mn-O bond distance, is only weakly affected.

In order to assess to what extent the d-p hoppings in the JT distorted structure are simply determined by the corresponding Mn-O distances, we also calculate MLWFs for $LaMnO_3$ in the undistorted simple cubic perovskite structure (i.e., with all three distortions discussed in Sec. II A deactivated) with different lattice constants a. The Mn-O distances in the cubic structures with $a = a_0 \pm \Delta a$ are identical to the long/short Mn-O bond length in the JT distorted structure with $Q^x = \Delta a/\sqrt{2}$. The corresponding results for the nearest neighbor hopping amplitudes between Mn(d) and O(p) orbitals are also shown in Fig. 5.

It is apparent that the $t_{t2g,p\pi}$-type hopping amplitudes in the JT distorted structures are nearly identical to the corresponding hopping amplitude in the undistorted cubic structure with the same Mn-O distance. The small deviations between these two cases as well as the weak effect of the JT distortion on the $t_{t2g,p\pi}$ hopping along z are due to changes in the orbital character of the MLWFs with increasing JT distortion. Thus, the magnitudes of the various hopping amplitudes are indeed determined mostly by the corresponding Mn-O bond lengths.

The case of the $t_{eg,p\sigma}$ hopping is only slightly different. The hopping (both in-plane and along z) between the Mn($3z^2 - r^2$)-type orbital and the surrounding O(p_σ) orbitals compares well with the hopping amplitude in the undistorted structure with the same Mn-O distance (even though the agreement for the short Mn-O distance is not as good as for $t_{t2g,p\pi}$). On the other hand, the JT-induced splitting of the in-plane hopping between the Mn($x^2 - y^2$)-type orbital and the surrounding O(p) orbitals is significantly weaker than the corresponding bond-length dependence in the cubic structure. This indicates a strong change of the $|x^2 - y^2\rangle$-type orbital with increasing JT distortion. This change is due to different admixture of other orbitals that are not explicitly included in the MLWF construction, i.e., O(s) and La(p), which lead to a reduction/expansion of the lobes directed along the shorter/longer Mn-O bonds with increasing JT distortion. This partially compensates the effect of changing Mn-O distance and leads to the observed JT dependence of the hopping.

C. Effect of U within the d-p model

In order to investigate the influence of the Hubbard U parameter on the TB parametrization obtained from the MLWFs, we now perform GGA+U calculations for the fully JT distorted structure and FM order using different values for U. Figure 6 shows the resulting U dependence of the on-site MLWF matrix elements. It can be seen that the diagonal elements (on-site energies ε) corresponding to O(p)-type MLWFs are virtually unaffected by the value of U, while the corresponding matrix elements for Mn(t_{2g}) and Mn(e_g) orbitals exhibit a more or less linear dependence on U.

This linear dependence is a direct consequence of the U-dependent potential shift applied to the TM d states within the DFT "+U" approach:[20]

$$\Delta V^{\sigma}_{mm'} = U\left(\frac{\delta_{mm'}}{2} - n^{\sigma}_{mm'}\right). \quad (6)$$

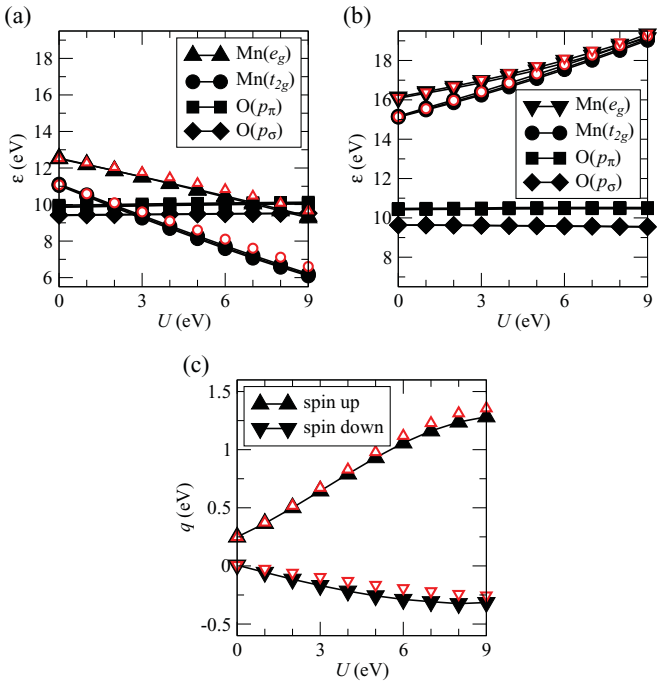

FIG. 6. (Color online) On-site energies corresponding to the d-p model as a function of Hubbard U for majority spin (a) and minority spin (b). (c) U dependence of the on-site off-diagonal elements q. The small open (red) symbols represent the GGA+U potential shifts added to the corresponding MLWF on-site matrix elements for $U = 0$.

Here, $n^{\sigma}_{mm'}$ is the occupation matrix element between atomic orbitals m and m' for spin projection σ, which is calculated from the projection of the occupied Bloch states on fixed atomic orbitals.

In order to quantify whether the U dependence of the on-site MLWF matrix elements does indeed correspond to this potential shift, we explicitly evaluate Eq. (6) for each U, using the atomic occupation matrix elements obtained from the corresponding GGA+U calculation, and add the so-obtained shifts to the on-site MLWF matrix elements for $U = 0$ eV. The resulting data is shown as small open (red) symbols in Fig. 6 and are nearly identical to the MLWF matrix elements calculated for the corresponding values of U. Thus, the GGA+U potential shifts are directly reflected in the on-site matrix elements of the MLWFs.

The reason for this good correspondence between the GGA+U potential shifts and the U dependence of the on-site MLWF matrix elements is the fact that the MLWFs of the extended d-p model are rather similar to the atomic orbitals used as projector functions within the GGA+U approach. To further demonstrate this similarity, we also compare the occupation matrix elements used to evaluate the GGA+U potential shifts with the occupation of the corresponding MLWFs:[35]

$$n^{\mathrm{MLWF}}_{mm'} = \int_{-\infty}^{E_{\mathrm{F}}} d\epsilon \int_{\mathrm{BZ}} d\mathbf{k} \sum_{l} \left(U^{(\mathbf{k})}_{lm}\right)^{*} \delta(\epsilon - \epsilon_{l\mathbf{k}})\, U^{(\mathbf{k})}_{lm'}, \qquad (7)$$

where E_{F} is the Fermi energy. The corresponding values for $U = 0$ eV are listed in Table I. It is apparent that the occupations of the MLWFs are very similar to the occupations

TABLE I. Average occupations n^{σ}_{mm} corresponding to Mn(t_{2g}) and Mn(e_g) orbitals calculated for $U = 0$ in the fully JT distorted structure. Rows denoted "Atomic" correspond to the fixed atomic orbitals used to evaluate the GGA+U functional; rows denoted "MLWF" contain the occupation of the MLWFs calculated according to Eq. (7); rows denoted "Formal" correspond to the ionic limit based on a high-spin d^4 configuration of the Mn cation. The last column contains the off-diagonal occupation matrix element $n^{\sigma}_{mm'}$ between the two different e_g orbitals. The first/last three rows correspond to majority/minority spin.

	σ	t_{2g}	e_g	e_g off diagonal
Atomic	↑	0.99	0.72	−0.11
MLWF	↑	1.00	0.68	−0.13
Formal	↑	1.0	0.5	
Atomic	↓	0.11	0.22	0.03
MLWF	↓	0.11	0.15	0.02
Formal	↓	0.0	0.0	

of the atomic orbitals used as GGA+U projector functions. Furthermore, we note that due to the strong hybridization between the Mn(d) and O(p) states, the occupation of the atomic-like d orbitals are quite different from a naïve expectation based on the formal ionic configuration of the Mn^{3+} cation.

The U dependence of the on-site off-diagonal matrix element q can be understood in the same way and is related to the off-diagonal occupation matrix element $n^{\sigma}_{mm'}$, where $m \mathrel{\widehat{=}} |3z^2 - r^2\rangle$ and $m' \mathrel{\widehat{=}} |x^2 - y^2\rangle$. The nonlinearities that can be observed for large U are due to changes in the corresponding $n^{\sigma}_{mm'}$. Note that since q is directly related to the JT splitting, increasing U effectively amounts to increasing the strength of the JT coupling. This is consistent with the fact that the (LDA/GGA)+U approach stabilizes the JT distortion compared to pure LDA/GGA.[29,36]

The U dependence of the hopping amplitudes between O(p)- and Mn(d)-like MLWFs for majority spin and FM order is shown in Fig. 7. All depicted hopping amplitudes exhibit a similar small increase in magnitude. The effect of U on the hopping amplitudes for minority spin (not shown) is even weaker than for the majority spin orbitals. These small changes in the hopping amplitudes for both majority and minority

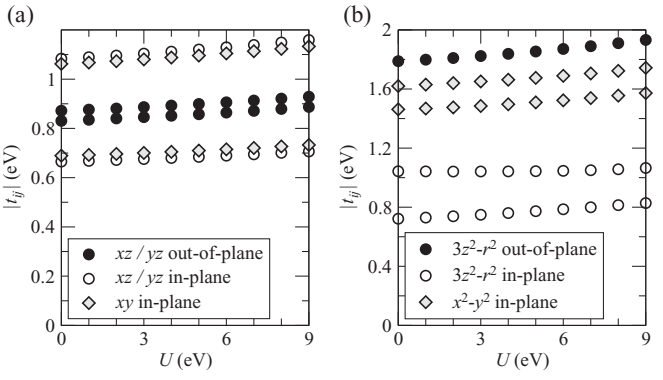

FIG. 7. Magnitude of hopping amplitudes between Mn(d) and O(p) nearest neighbor orbitals as function of the Hubbard U. (a) $t_{2g} - p_\pi$ hoppings. (b) $e_g - p_\sigma$ hoppings. Notation is the same as in Fig. 5.

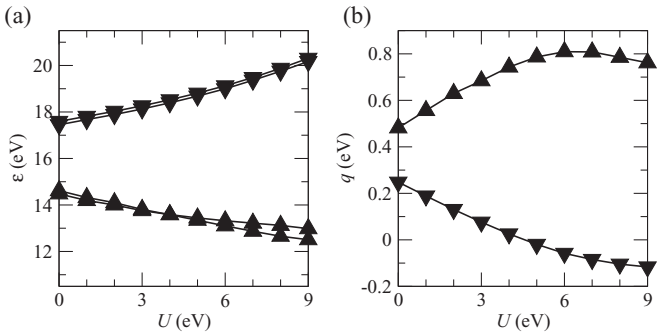

FIG. 8. On-site energies ε (a) and on-site off-diagonal matrix element q (b) of the effective e_g MLWF parametrization as function of the Hubbard U. Majority spin and minority spin are denoted by up and down triangles, respectively.

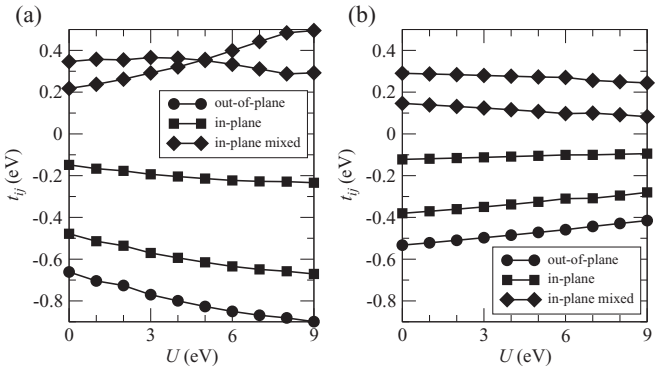

FIG. 9. Effect of U on the nearest neighbor hopping amplitudes of the effective e_g MLWFs for majority spin (a) and minority spin (b). "In-plane" and "out-of-plane" correspond to hopping between similar orbitals within the x-y plane and along z, respectively, while "in-plane mixed" denotes the hopping between two different e_g MLWFs at neighboring sites within the x-y plane.

spin can be attributed to changes in orbital character of the corresponding MLWFs. These changes in orbital character arise from a different admixture (hybridization) of orbitals centered at the surrounding ions, which results from the U-dependent shifts of the on-site energies of the Mn(d) states relative to all other orbitals.

D. Effect of U within the effective e_g model

We now contrast the U dependence of the TB parameters for the extended d-p model presented in the previous section with the case of an effective e_g model with only two e_g-like Wannier orbitals on each Mn site. This is probably the most common model used to describe the physics of manganites (see, e.g., Ref. 3), and a detailed analysis of the effect of various distortions and different magnetic arrangements on the corresponding MLWF matrix elements for $U = 0$ eV has been presented in Ref. 11. Here we focus on changes in the MLWF parametrization due to the Hubbard U correction for the purely JT distorted structure and FM order. The corresponding Wannier functions are constructed from the Kohn-Sham states located within an energy window of 12.0–17.0 eV and 15.9–20.0 eV for majority and minority spin, respectively. For further details see Ref. 11.

Figure 8 shows the U dependence of the on-site MLWF Hamiltonian matrix elements for the effective e_g model. It can be seen that in particular the on-site energies exhibit a very similar trend to the on-site energies of the e_g-like MLWFs in the d-p model, but that the U dependence is weaker than in the latter case. The slope $d\varepsilon/dU$ for both majority and minority spin is only about 66% compared to the d-p model. This indicates that the U dependence of the on-site energies for the effective e_g MLWFs is still determined by the GGA+U potential shifts, Eq. (6), but is renormalized by the extent of overlap between the extended MLWF and the corresponding e_g atomic orbital. In other words, the U-dependent energy shift experienced by the MLWF is determined by the projection of the MLWF on atomic orbitals and the occupation of these atomic orbitals.

In particular, this shows that the effect of U on the on-site energies of the effective e_g MLWFs is *not* determined by the occupation of the MLWFs themselves via a relation similar to Eq. (6). The occupation of the effective e_g MLWFs is essentially identical to the "formal" occupations listed in Table I, corresponding to the formal 3+ charge state of the Mn cation in $LaMnO_3$ (0.5 for majority spin and 0.0 for minority spin). Therefore, the occupation-dependent potential shift following from a mean-field approximation to the Hubbard interaction similar to Eq. (6) would be zero for the majority spin e_g states.[37] The U dependence of the corresponding on-site energies is thus notably different from a mean-field treatment of the electron-electron interaction in a two-orbital Hubbard-like model derived from the effective e_g TB parametrization.

We point out that in addition to the different dependence on orbital occupation, the magnitude of the screened Hubbard U acting on the extended e_g-like Wannier orbitals will of course be significantly reduced compared to the magnitude of U corresponding to more localized atomic-type orbitals. A comparison of the value of U for "atomic-like" and "effective" Wannier orbitals in an Fe-pnictide system based on calculations using the constrained random phase approximation has been presented recently in Ref. 38.

Similar to the case of the on-site energies, the U dependence of the off-diagonal on-site matrix elements q, shown in Fig. 8(b), resembles the U dependence of the corresponding atomic-like MLWFs shown in Fig. 6(c). The decrease of q for majority spin observed for $U > 6$ eV can then be ascribed to changes in orbital character of the extended MLWFs, which lead to different projections between MLWFs and the corresponding atomic orbitals.

Finally, Fig. 9 shows the U dependence of the nearest neighbor hopping parameters for the effective e_g MLWFs. For majority spin, there is an overall increase in the magnitude of the hopping, whereas for minority spin there is an overall decrease. Compared to the d-p model discussed in the previous section, the effect of U on the hopping amplitudes of the effective e_g model is strongly enhanced, with typical changes between 30% and 60% over the considered range of U values. For the in-plane hopping between $|3z^2 - r^2\rangle$- and $|x^2 - y^2\rangle$-type orbitals the change can be even more than 100%.

This strong effect of U on the hopping amplitudes of the effective e_g MLWFs can be explained by the changes in the

underlying d-p model. The effective e_g MLWFs are essentially linear combinations of an atomic-like Mn(e_g) orbital and O(p_σ) orbitals on the surrounding anions. As demonstrated in the previous section, the on-site energies of the atomic d orbitals are strongly shifted relative to the oxygen p orbitals as a function of U. This shift affects the hybridization between the atomic orbitals and thus changes the admixture of O(p_σ) orbitals in the effective e_g MLWF. For majority spin, increasing U decreases the energy difference between atomic O(p) and Mn(d) orbitals and thus increases the hybridization, i.e., the admixture of O(p) in the effective e_g MLWF. This leads to an increase of the hopping amplitude due to the larger overlap between effective e_g orbitals at neighboring Mn sites. For minority spin the trend is opposite to this, resulting in the decrease in magnitude seen in Fig. 9(b).

Considering a simple d-p nearest neighbor TB model for the cubic perovskite structure, one can show that in the limit of large energy separation between the d and p orbitals, the "antibonding" bands that result from the d-p hybridization are formally equivalent to an effective "d-only" TB model with direct hopping between d orbitals on adjacent TM sites. The amplitude of this "effective" d-d hopping is thereby given as

$$t_{dd}^{\text{eff}} = \frac{t_{dp}^2}{\varepsilon_d - \varepsilon_p}. \tag{8}$$

Obviously, the overall trends discussed in the previous paragraph are consistent with this simple picture, but the limit for which Eq. (8) is valid is not fulfilled in the case of $LaMnO_3$. This is apparent from the on-site energies shown in Fig. 6(a), where it can be seen that for values of U larger than 5–6 eV the Mn(e_g) states become essentially degenerate with the O(p) states. We also verified that Eq. (8) is not fulfilled quantitatively by the hoppings calculated from both sets of MLWFs (d-p and effective e_g). Thus, even though it is possible to obtain a reasonable MLWF parametrization of the effective e_g bands for all values of U, it is not obvious whether a low-energy description of $LaMnO_3$ based only on effective e_g states is always physically reasonable. We note that values of $U \approx 9$ eV and $U - J = 4.5$ eV have been calculated for $LaMnO_3$ in Refs. 39 and 40, respectively, using different methods. Furthermore, an optimal value of $U = 5.5$ eV has been suggested in Ref. 41.

The partial "breakdown" of the effective e_g description of $LaMnO_3$ for values of U larger than 5–6 eV also leads to a strong dependence of some MLWF parameters on subtle differences in the underlying Kohn-Sham band structure. For example the "crossing" of the mixed in-plane hopping amplitudes, i.e. corresponding to the in-plane hopping between $|3z^2 - r^2\rangle$- and $|x^2 - y^2\rangle$-type orbitals, that can be seen around $U = 5$ eV in Fig. 9(a), appears only if orthogonalized atomic orbitals are used to evaluate the "$+U$" correction to the GGA energy functional. If instead a projection on nonorthogonal atomic orbitals is used (option "atomic" instead of "ortho-atomic" within QUANTUM ESPRESSO), the resulting MLWF matrix elements do not exhibit this feature.

IV. SUMMARY AND CONCLUSIONS

In summary, we have discussed differences in the MLWF-derived TB parametrization of $LaMnO_3$ that result from different values of the Hubbard U used in the GGA+U calculation from which the MLWFs are obtained. Thereby, we have compared two different ways to represent the important bands around the Fermi energy. First, a d-p *TB model* based on atomic-like Mn(d) and O(p) MLWFs, and second, an *effective* e_g *TB model* involving only two e_g-like Wannier orbitals per Mn.

We have shown that the hopping amplitudes of the d-p model are only weakly affected by a variation of U, and that the resulting changes in the on-site Hamiltonian matrix elements are consistent with a mean-field approximation to the electron-electron interaction for the corresponding TB Hubbard Hamiltonian. As a result, the TB parameters for the d-p model of $LaMnO_3$ are fairly insensitive to variations of U and can therefore be determined accurately without detailed knowledge about the precise value of U for the corresponding d orbitals.

In contrast, the hopping amplitudes for the effective e_g TB parametrization depend strongly on the value of U used in the GGA+U calculation. This is due to pronounced changes in the amount of admixture of O(p) ligand orbital character in the effective e_g MLWFs, which in turn is due to the large U-dependent shifts of the on-site energies of the corresponding atomic orbitals. Furthermore, the U dependence within a mean-field Hubbard Hamiltonian derived from the effective e_g MLWF parameters is distinctly different from the U dependence of the MLWF parameters themselves. The former is determined by the occupations of the effective e_g orbitals and the value of the screened Hubbard interaction in that basis, whereas the latter is determined by the occupations and the value of the screened Hubbard interaction corresponding to atomic-like d states. A determination of suitable TB parameters for an effective e_g model of $LaMnO_3$ therefore requires an accurate knowledge of U in both basis sets. This is particularly important for the determination of the JT coupling strength, which is determined from the on-site splitting within the e_g orbital manifold. This splitting on the other hand is critically affected by the value of U in both the GGA+U calculation and the mean-field Hubbard Hamiltonian.

In addition to the U dependence, we have also analyzed the effect of the staggered JT distortion ("Q^x-type") on the TB parametrization of the d-p model. We have found that the JT distortion manifests itself both as a local ligand-/crystal-field splitting within the e_g orbital manifold, as well as via a pronounced bond-length dependence of the nearest neighbor d-p hopping amplitudes. Our results demonstrate that even for the rather localized atomic-like d-p MLWFs, the ligand-field effect dominates over the purely electrostatic crystal-field effect. Furthermore, we have verified that the changes in the nearest neighbor hopping amplitudes due to the JT distortion are almost fully determined by the resulting change in Mn-O bond length.

A number of more general conclusions can be drawn from the results obtained in this work. It is reasonable to assume that the sensitivity/insensitivity of certain MLWF parameters from the specific value of U used in the GGA+U calculation can be generalized to a general sensitivity/insensitivity from the choice of exchange-correlation functional used in the electronic structure calculation. In the present study, we made use of the similarity between the "$+U$" correction to the GGA

functional and the mean-field approximation to the electron-electron interaction in the corresponding model Hamiltonian (assuming of course that the latter is described via a local Hubbard interaction). Using this similarity, the observed trends in the MLWF TB parameters and the difference between the two different TB models can be explained. The same similarity between DFT and mean-field Hubbard model is not present if the electronic structure is calculated using other "beyond LDA/GGA" methods such as for example self-interaction corrected methods,[17] hybrid functionals,[21] or the GW approach.[42] In these cases the electronic band structure should also be compared with the mean-field approximation of an appropriate TB Hamiltonian. To extract the "bare" or "noninteracting" on-site energies and off-diagonal on-site matrix elements, one has to then subtract a U-dependent shift similar to Eq. (6). The corresponding value of U has to be calculated by other means, for example via the recently proposed approach based on the constrained random phase approximation.[43,44]

While the so-obtained TB models will always give an essentially perfect representation of the Kohn-Sham bands for the given reference, it is still important to test whether the corresponding parametrization is also transferable to slightly different configurations, i.e., with different structural distortions and/or magnetic/orbital order. Of course, as shown through the comparison between the effective e_g and the more elaborate d-p model for $LaMnO_3$, transferability can always be improved by including more orbitals in the TB basis set.

Finally, we note that in the present work we have focused on how to obtain TB parameters using the DFT Kohn-Sham band structure as (mean-field) reference. An entirely different, albeit at least equally important, question is whether these bands, calculated using a suitable exchange-correlation functional for a particular system, are indeed a good representation of the real material. However, this question is beyond the scope of the present study and will most likely be the topic of future research for a number of years to come.

V. ACKNOWLEDGMENTS

This work was supported by Science Foundation Ireland under Ref. SFI-07/YI2/I1051 and made use of computational facilities provided by the Trinity Center for High Performance Computing. We also acknowledge partial support by the EU-FP7 project ATHENA.

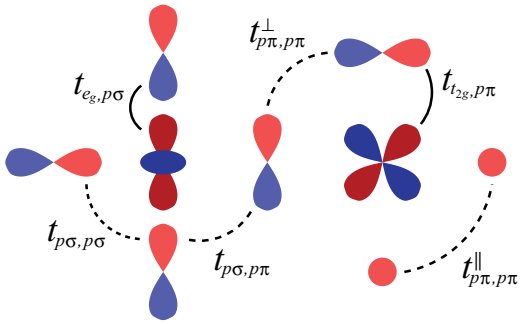

FIG. 10. (Color online) Schematic depiction of all closest neighbor Mn-O and O-O hopping amplitudes within the extended d-p model of $LaMnO_3$.

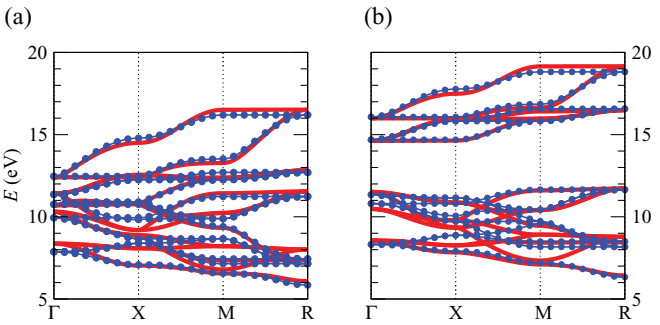

FIG. 11. (Color online) Band dispersion calculated from the MLWFs (thick line) and from the truncated TB model described in the main text (dots and line). (a) Majority spin. (b) Minority spin.

APPENDIX: FURTHER DETAILS ON THE d-p TB PARAMETRIZATION FOR CUBIC $LaMnO_3$

In this appendix we give a more quantitative account of the d-p TB parametrization obtained from the MLWFs for simple cubic $LaMnO_3$ and FM order.

There are 2 different hopping parameters between nearest neighbor Mn(d) and O(p) states ($t_{eg,p\sigma}, t_{t2g,p\pi}$) and 4 independent hopping parameters between closest neighbor O(p) states ($t_{p\sigma,p\sigma}, t_{p\sigma,p\pi}, t^{\perp}_{p\pi,p\pi}, t^{\parallel}_{p\pi,p\pi}$) that are allowed by the symmetry of the system. All of these hopping parameters are illustrated in Fig. 10. The corresponding values together with the various on-site energies are summarized in Table II. It can be seen that the minority spin hopping amplitudes corresponding to nearest neighbor d-p hopping are slightly larger than for majority spin, whereas the opposite is the case for the closest neighbor p-p hoppings (except for $t^{\parallel}_{p\pi,p\pi}$).

Within the two-center approximation to the linear combination of atomic orbitals (LCAO) method all closest neighbor O(p)-O(p) hoppings can be expressed as a linear combination of purely σ- and π-type hopping parameters, $t(pp\sigma)$ and $t(pp\pi)$.[45] Thereby, $t(pp\pi)$ corresponds directly to $t^{\parallel}_{p\pi,p\pi}$ in our notation. Calculating an estimate for $t(pp\sigma)$ from each of the remaining MLWF hopping parameters as ($t^{\parallel}_{p\pi,p\pi} - 2t_{p\sigma,p\sigma}$), ($t^{\parallel}_{p\pi,p\pi} - 2t^{\perp}_{p\pi,p\pi}$), or ($-t^{\parallel}_{p\pi,p\pi} + 2t_{p\sigma,p\pi}$), we obtain

TABLE II. On-site energies and nearest neighbor Mn-O and O-O hopping amplitudes obtained for the d-p MLWFs in the cubic structure with FM order. In addition, the hopping between t_{2g} orbitals along the shortest Mn-Mn distance is also listed. All values are given in eV.

	Majority spin	Minority spin
ε[Mn(e_g)]	12.459	16.074
ε[Mn(t_{2g})]	11.031	15.104
ε[O(p_σ)]	9.400	9.603
ε[O(p_π)]	9.888	10.432
$t_{eg,p\sigma}$	1.768	1.861
$t_{t2g,p\pi}$	−0.852	−0.982
$t_{p\sigma,p\sigma}$	−0.444	−0.409
$t_{p\sigma,p\pi}$	0.306	0.265
$t^{\perp}_{p\pi,p\pi}$	−0.337	−0.304
$t^{\parallel}_{p\pi,p\pi}$	−0.014	−0.092
$t_{t2g,t2g}$	−0.069	−0.105

values of 0.873/0.725 eV, 0.660/0.516 eV, or 0.627/0.622 eV, for majority/minority spin, respectively. The spread in these values shows to what extent the approximation of rigid atomic orbitals is not fulfilled within the d-p set of MLWFs.

In a previous study, LCAO parameters for manganites were deduced based on a cluster-model analysis of photoemission spectra,[46] leading to the following values for the hopping integrals: $t(pd\sigma) = 1.8$ eV, $t(pd\pi) = 0.9$ eV, $t(pp\sigma) = 0.60$ eV, $t(pp\pi) = -0.15$ eV. These values are in reasonable agreement with the values obtained from the MLWFs listed in Table II.

In Fig. 10 we show a comparison of the dispersion between the MLWF bands and a 14-band TB model calculated using the parameters given in Table II, i.e., by neglecting all other further neighbor hoppings. The overall band dispersion is rather well reproduced in the truncated TB model. However, due to a rather slow decay of hopping amplitudes with further neighbor distance, certain features are not reproduced. In addition, neglecting further-neighbor hoppings also leads to a slight underestimation of the total bandwidth in the truncated TB model. We find that there are overall 14 different further neighbor hoppings with magnitudes in the range of (0.020–0.113) eV. Out of these only the direct hopping between neighboring t_{2g} orbitals (last line in Table II) leads to a significant improvement of the TB bands and is therefore included in Table II.

*kovacikr@tcd.ie

[1] E. Dagotto, Rev. Mod. Phys. **66**, 763 (1994).
[2] M. Imada, A. Fujimori, and Y. Tokura, Rev. Mod. Phys. **70**, 1039 (1998).
[3] E. Dagotto, T. Hotta, and A. Moreo, Phys. Rep. **344**, 1 (2001).
[4] P. Hohenberg and W. Kohn, Phys. Rev. **136**, B864 (1964).
[5] W. Kohn and L. J. Sham, Phys. Rev. **140**, A1133 (1965).
[6] O. Gunnarsson, O. K. Andersen, O. Jepsen, and J. Zaanen, Phys. Rev. B **39**, 1708 (1989).
[7] M. S. Hybertsen, M. Schlüter, and N. E. Christensen, Phys. Rev. B **39**, 9028 (1989).
[8] L. Hozoi, U. Birkenheuer, P. Fulde, A. Mitrushchenkov, and H. Stoll, Phys. Rev. B **76**, 085109 (2007).
[9] R. Bastardis, C. de Graaf, and N. Guihéry, Phys. Rev. B **77**, 054426 (2008).
[10] C. Ederer, C. Lin, and A. J. Millis, Phys. Rev. B **76**, 155105 (2007).
[11] R. Kováčik and C. Ederer, Phys. Rev. B **81**, 245108 (2010).
[12] T. F. A. Müller, V. Anisimov, T. M. Rice, I. Dasgupta, and T. Saha-Dasgupta, Phys. Rev. B **57**, 12655 (1998).
[13] W. Ku, H. Rosner, W. E. Pickett, and R. T. Scalettar, Phys. Rev. Lett. **89**, 167204 (2002).
[14] E. Zurek, O. Jepsen, and O. K. Andersen, ChemPhysChem **6**, 1934 (2005).
[15] F. Lechermann, A. Georges, A. Poteryaev, S. Biermann, M. Posternak, A. Yamasaki, and O. K. Andersen, Phys. Rev. B **74**, 125120 (2006).
[16] I. V. Solovyev, Phys. Rev. B **73**, 155117 (2006).
[17] J. P. Perdew and A. Zunger, Phys. Rev. B **23**, 5048 (1981).
[18] J. P. Perdew, K. Burke, and M. Ernzerhof, Phys. Rev. Lett. **77**, 3865 (1996).
[19] A. I. Liechtenstein, V. I. Anisimov, and J. Zaanen, Phys. Rev. B **52**, 5467 (1995).
[20] S. L. Dudarev, G. A. Botton, S. Y. Savrasov, C. J. Humphreys, and A. P. Sutton, Phys. Rev. B **57**, 1505 (1998).
[21] A. D. Becke, J. Chem. Phys. **98**, 1372 (1993).
[22] N. Marzari and D. Vanderbilt, Phys. Rev. B **56**, 12847 (1997).
[23] I. Souza, N. Marzari, and D. Vanderbilt, Phys. Rev. B **65**, 035109 (2001).
[24] A. A. Mostofi, J. R. Yates, Y.-S. Lee, I. Souza, D. Vanderbilt, and N. Marzari, Comput. Phys. Commun. **178**, 685 (2008).
[25] J. M. D. Coey, M. Viret, and S. v. Molnár, Adv. Phys. **48**, 167 (1999).
[26] J. B. A. A. Elemans, B. V. Laar, K. R. V. d. Veen, and B. O. Loopstra, J. Solid State Chem. **3**, 238 (1971).
[27] W. E. Pickett and D. J. Singh, Phys. Rev. B **53**, 1146 (1996).
[28] S. Satpathy, Z. S. Popović, and F. R. Vukajlović, Phys. Rev. Lett. **76**, 960 (1996).
[29] H. Sawada, Y. Morikawa, K. Terakura, and N. Hamada, Phys. Rev. B **56**, 12154 (1997).
[30] P. Giannozzi *et al.*, J. Phys. Condens. Matter **21**, 395502 (2009).
[31] D. Vanderbilt, Phys. Rev. B **41**, 7892 (1990).
[32] P. Norby, I. K. Andersen, E. K. Andersen, and N. Andersen, J. Solid State Chem. **119**, 191 (1995).
[33] A. Kokalj, Comput. Mater. Sci. **28**, 155 (2003); code available from [http://www.xcrysden.org/].
[34] J. Kanamori, J. Appl. Phys. (Suppl.) **31**, 14 (1960).
[35] For simplicity of notation we suppress the spin index σ here. It should be understood that in general the eigenvalues $\epsilon_{l\mathbf{k}}$, the unitary matrices $\mathbf{U}^{(\mathbf{k})}$, and the occupation matrix of the MLWFs can be spin dependent.
[36] W.-G. Yin, D. Volja, and W. Ku, Phys. Rev. Lett. **96**, 116405 (2006).
[37] We point out that Eq. (6) corresponds to a simplified Hubbard interaction with exchange parameter $J = 0$. While for a more general interaction with $J \neq 0$ the potential shifts would be different, our general conclusion would be unaffected. For simplicity of presentation we therefore only discuss the case $J = 0$.
[38] M. Aichhorn, L. Pourovskii, V. Vildosola, M. Ferrero, O. Parcollet, T. Miyake, A. Georges, and S. Biermann, Phys. Rev. B **80**, 085101 (2009).
[39] I. Solovyev, N. Hamada, and K. Terakura, Phys. Rev. B **53**, 7158 (1996).
[40] G. Trimarchi and N. Binggeli, Phys. Rev. B **71**, 035101 (2005).
[41] Z. Yang, Z. Huang, L. Ye, and X. Xie, Phys. Rev. B **60**, 15674 (1999).
[42] F. Aryasetiawan and O. Gunnarsson, Rep. Prog. Phys. **61**, 237 (1998).
[43] F. Aryasetiawan, M. Imada, A. Georges, G. Kotliar, S. Biermann, and A. I. Lichtenstein, Phys. Rev. B **70**, 195104 (2004).
[44] T. Miyake and F. Aryasetiawan, Phys. Rev. B **77**, 085122 (2008).
[45] J. C. Slater and G. F. Koster, Phys. Rev. **94**, 1498 (1954).
[46] T. Mizokawa and A. Fujimori, Phys. Rev. B **54**, 5368 (1996).